

You Are Here: Geolocation by Embedding Maps and Images

Obed Samano Abonce, Mengjie Zhou and Andrew Calway
 Department of Computer Science
 University of Bristol

{os17592, mengjie.zhou, andrew.calway}@bristol.ac.uk

April 15, 2022

Abstract

We present a novel approach to geolocating images on a 2-D map based on learning a low dimensional embedded space, which allows a comparison between an image captured at a location and local neighbourhoods of the map. The representation is not sufficiently discriminatory to allow localisation from a single image but when concatenated along a route, localisation converges quickly, with over 90% accuracy being achieved for routes up to 200m in length when using Google Street View and Open Street Map data. The approach generalises a previous fixed semantic feature based approach and achieves faster convergence and higher accuracy without the need for including turn information.

1 Introduction

We consider the problem of geolocating images on a 2-D cartographic map without using GPS. Instead, as illustrated in Fig. 1, we seek to link the semantic information on the map to the content in the image, hence localising the latter. This is akin to the human skill of interpreting maps for way-finding (reading a map), using for example detailed survey maps or the ubiquitous You Are Here schematic maps found in cities and tourist attractions. It is similar in nature to the visual place recognition problem, which has attracted significant interest in computer vision and robotics [17], but differs in that the ‘reference’ is a 2-D map rather than a large database of geolocated images.

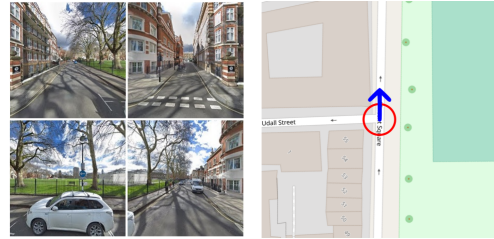


Figure 1: Images (left) were taken in different directions at the location circled in the map (right), where the arrow indicates the forward direction (top left image). The junction, buildings and green areas on the map are clearly visible in the image, illustrating the semantic features that we seek to leverage for geolocation.

Our motivation is multifold. In addition to removing reliance on positioning infrastructure such as GPS, the use of compact and readily available map data has the potential to address the scalability problems associated with solutions employing geolocated images, which have large memory requirements and significant data acquisition logistics. We also envisage that techniques for representing and understanding spatial semantics will likely be needed as human-robot interaction becomes increasingly sophisticated. For example, by endowing autonomous systems with the ability to produce convincing visual and/or oral descriptions to aid in human way-finding.

We adopt a learning approach, building upon and generalising the semantic feature approach proposed by Panphattarasap and Calway [22]. Locations are represented in

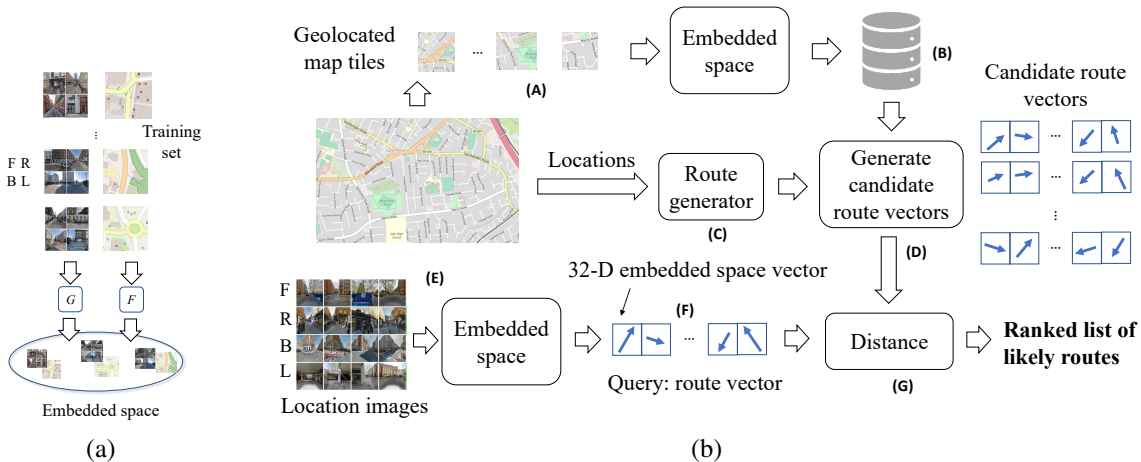


Figure 2: Overview: (a) we learn transformations G and F which embed location images (in four directions - F, R, B and L) and map tiles, respectively, into a low dimensional vector space (32-D), within which corresponding image/map tile pairs are close; (b) Embedded representations are computed for all map tiles (A) and stored with their locations (B), for given route length, all potential routes are computed (C) and corresponding route vectors are generated from the map tile vectors (D), embedded representations are computed for images captured along test route (E) giving a query route vector (F) which is compared with all potential route vectors derived from the map (G), resulting in a ranked list of likely routes.

the latter by binary descriptors indicating the presence or not of pre-selected semantic features (junctions and gaps between buildings), limiting applicability to areas rich in those features and for which they provide sufficient discrimination. In contrast, we seek to learn descriptions which optimally link images to local map areas, without pre-assumptions as to which map features are important, with the dual aim of generalising and increasing discrimination.

We learn a relationship between location images and map tiles (corresponding to neighbourhoods around locations) by deriving a low dimensional embedded vector space (32-D in this work) within which corresponding image and map tile pairs are close, see Figure 2a. We use images from Google Street View (GSV) and map tiles from Open Street Map (OSM) as training data and a siamese-like learning network architecture with triplet loss function to derive the embedded space. This provides a means of assessing similarity between an image and potential map locations. However, in common with that in [22], the representation is not sufficiently discriminatory to localise from a single image (many places share similar map

tiles).

Instead, analogous to the approach in [22], it is the pattern of embedded vectors along distinct routes which facilitates localisation, with the required length of route dependent on local semantic characteristics. Localisation therefore proceeds by transforming the sequence of images captured along a route into the embedded space and comparing the concatenated vectors with those derived from sequences of map tiles computed along all routes within the 2-D map, yielding a ranked list of likely locations and routes. Figure 2b provides a schematic overview of the approach. In summary, we demonstrate the following key findings:

1. It is possible to learn an embedded vector space which provides a means of linking the semantics of local map tiles with image content.
2. The resulting embedded space can be used to geolocate sequences of images along a route, achieving up to 90% success rate for routes of around 200 m within a 2.5km² area.

3. The embedded space approach results in a significant increase in success rates for shorter routes and avoids the need for incorporating turn information compared to the approach used in [22]. This demonstrates its ability to generalise and to increase discrimination.

In the next section we discuss related work, followed in Section 3 by details of the architecture and learning framework used to derive the embedded space. Section 4 gives details of the localisation framework. Section 5 shows results of experiments using GSV and OSM data, including a comparison of performance with the method used in [22].

2 Related Work

A key insight identified in [22] is that map semantics along a route provides a means of uniquely identifying location. A minimal 4-bit descriptor indicating the presence or not of semantic features is used to characterise locations (junctions to the front and rear and gaps between buildings to the left and right) and convolutional neural network (CNN) classifiers trained on GSV/OSM data are used to determine feature presence and estimate descriptors from 360 degree images. Descriptors are then concatenated along routes to allow localisation by comparison with a database of route descriptors derived from the map. Accuracy of 85% is reported for test routes up to 200m in length using GSV/OSM data when descriptors are combined with left/right turn information along routes, although this dropped to 45% when turn information was not used. The same 4-bit descriptors are also used in a particle filtering implementation in [30], although results suggest that localisation is slower to converge, possibly due to the limited route memory within the filter.

Other related work which makes use of map data for localisation includes that reported in [9, 24, 5, 19, 11, 1, 18], all of which focus on its use for self-driving vehicle navigation. In [24], learning from GSV/OSM data is used to recognise semantic features in road scenes such as junctions, bike lanes, etc, to verify GPS positioning, whilst in [9] and [5] visual odometry is used to track location on a 2-D map by matching with road topology. This is ex-

tended in [19] to incorporate semantic cues such as sun direction, junctions and speed limits. End-to-end learning is adopted in [11, 1, 18], combining image data with road topology to predict steering control commands, trained using GPS and driver control execution data. Map semantics have also been used in conjunction with GPS to aid 6-D pose estimation from images, see e.g. [6, 4, 20, 3], although the focus in this work is on precise metric pose estimation as opposed to large scale geo-localisation.

Our approach to learning an embedded space is motivated in part by work matching aerial and street level images [16, 29, 27, 26, 13], and that reported in [25], which learns an embedded space for map tiles reflecting semantic similarity. In essence, we combine these two ideas, replacing the aerial images in the former by map tiles and using a siamese-like network architecture similar to that used in [13] to learn an embedded space which links location images to map tiles.

3 Embedding Maps and Images

In this section we describe the model, data sets and methodology used to learn an embedded space for location images and map tiles, within which semantically similar pairs are close. Our data inputs are panoramic images from GSV and RGB image tiles corresponding to local neighbourhoods of a 2-D map rendered from OSM.

3.1 Network Model

Our network architecture is shown in Figure 3. It has a siamese-like form, consisting of two independent sub-networks, one for location images and one for map tiles, each having a feature extractor and a projection module. We keep the weights in corresponding layers independent since each sub-network is processing information from very different domains.

In the location image sub-network, the feature extractor module is based on the Resnet50 architecture [10], from which we have removed the top layers and coupled a trainable NetVLAD layer [2] after the last convolution. The input to the module is four images corresponding to front, left, right and back views (w.r.t the vehicle heading direction) cropped from the GSV panoramic image. A descriptor vector for each view direction is generated and these

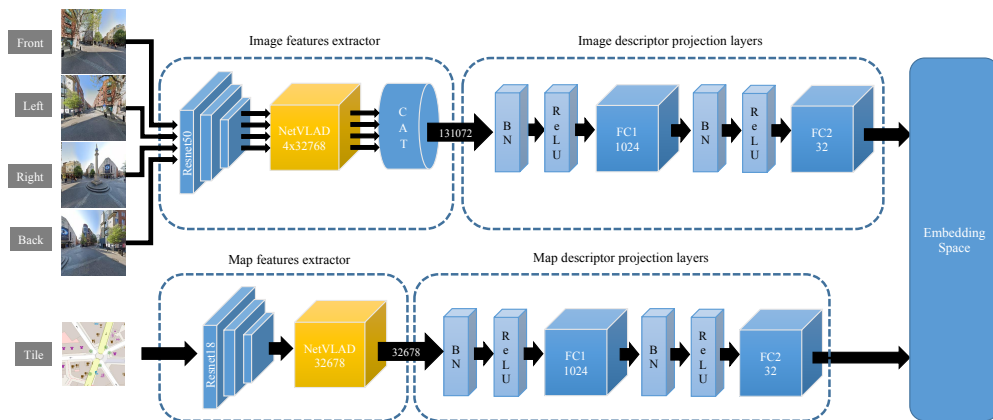


Figure 3: Network architecture for learning an embedded vector space within which corresponding location images (consisting of four - front, left, right and back - viewing directions) and map tiles are close. Each are processed independently via a sub-network consisting of feature extraction and projection layers, resulting in a 32-D embedded space. See text for further details.

are concatenated for input to the projection module. Similarly, the map tile feature extractor also uses a residual network architecture coupled to a NetVLAD layer. However, we use Resnet18 [10] in place of Resnet50, since map tiles contain considerably fewer details than the location images. The module input is a map tile corresponding to the same location from which the GSV panoramic was taken (for a given location we use two zoom levels - see below) and the output is a descriptor vector.

In both sub-networks, the projection module consist of two fully connected layers, both preceded by batch normalization [14] and ReLU activation [21], which reduce the dimensionality of the descriptors down to the embedding size (we used 32-D) and help to project semantically similar inputs near to each other.

3.2 Data sets

We used geolocated GSV panoramic images and map tiles rendered from OSM for both our training and test data sets. This enabled us to perform extensive experimentation to evaluate a proof of principle system. We are not aware of any publicly available data sets composed of aligned panoramas and map tiles and so we leave ‘in the wild’ evaluation for future work.

For the training set, from OSM, we extracted over

700,000 road nodes from six different cities across the U.K, including urban, suburban, and rural areas. We filtered the locations, keeping only those corresponding to drivable roads and excluded pedestrian, cycling, and other service paths. For each location, the nearest GSV panoramic image was downloaded according to its latitude and longitude, along with its vehicle heading direction (yaw). Finally, we rendered two 256x256 pixel map tiles, each with a different zoom level, for every location, with the tiles centred on the coordinates of the corresponding GSV panoramic images to ensure a geographic match between the data domains. The map projection was also rotated to align it with the GSV heading direction. We rendered at two different zoom levels to allow exploration of the effect of zoom in the model and also to provide data augmentation in the training process (see below). The result is a data set consisting of 731,960 panorama images and 1,463,920 map tiles, two tiles for each location.

For validation and testing, we created six further data sets, three from cities in the UK (London, Edinburgh and Luton) and three from cities outside of the UK (Paris, New York and Toronto). For testing we need to simulate an autonomous system moving along a route whilst collecting images at regular intervals. Hence, we generated data corresponding to adjacent locations at approximately 10 meter intervals. A summary of the testing data sets,

including the number of locations and approximate geographic extent, is given in Table 1. We reserved the Paris data set for training validation and used the rest of data sets for testing.

3.3 Training data

We trained our model in an end-to-end way as all network parameters, including feature extraction, NetVLAD and projection layers, are updated at the same time. Since we do not have categories, or equivalently every location is a category, we train the model using a self-supervised method based on triplet loss metric learning [23], similar to that used in [13]. Note that we have to take care when considering data augmentation, since we need to maintain position and point of view relationships between the two domains, e.g. warping a map tile would require a suitable transformation of the corresponding location images, which is non-trivial to compute. Hence we limit augmentation to small changes in the zoom of the map tiles and the viewing directions when cropping the panoramic images (see below). To form triplets, we take examples of matched and unmatched image/map tile pairs inside every batch.

We generate the matched pairs as follows. Let X and Y denote the set of training tiles and panoramic images, respectively, and let L be the set of all locations. We start the training process by taking n random locations to form a subset L_B of locations in the training batch. Then, for each location $l_i \in L_B$, we take the associated panoramic image $y_i \in Y$ and pick a map tile $x_i \in \{x_i^1, x_i^2\}$ at random, where x_i^1 and x_i^2 are the two map tiles at different zoom levels for location i . We then apply data augmentation to generate $1 \leq k \leq K$ different image/map tile pairs for each location l_i . Specifically, in the case of map tiles, we apply $T_x : x_i \rightarrow x_{ik}$, where T_x applies a further random small zoom to x_i and resizes it to 224x224 pixels, i.e. we randomly generate map tiles with random zoom levels around that of the two ‘reference’ tiles. In the case of the panoramic images, we apply $T_y : y_i \rightarrow y_{ik} = (y_{ik}^F, y_{ik}^L, y_{ik}^R, y_{ik}^B)$ that takes y_i and crops four 224x224 pixel images in the front, left, right and back viewing directions, respectively, relative to the vehicle heading direction, with a random component in the cropping parameters to provide a degree of visual variation. We denote y_{ik} as a ‘4-image’. In addition, we

Dataset	N	Area	Dataset	N	Area
Edinburgh	2522	2.6	New York	4185	1.9
London	5605	2.9	Paris	2563	1.4
Luton	3579	2.8	Toronto	8161	5.7

Table 1: Summary of validation and testing data sets, where N means the number of locations, and the area is given in km^2 . Except Luton, which is suburban, others are all urban areas.

incorporate a standard colour normalisation and a random vertical flip in both T_x and T_y .

In summary, at each training step, there are N_B locations in the batch, each with K 4-image/map tile pairs. This gives a total of $N_B K$ pairs, from which we can generate $N_B K^2$ matched pairs and $N_B(N_B - 1)K^2$ unmatched pairs. Hence, the ratio of matched versus unmatched pairs depends on the number of locations in the batch.

3.4 Loss function

For the loss function, we used the weighted soft-margin ranking loss proposed in [13], a variation of that in [27, 12] to address the problem of having to select the margin parameter in a traditional triplet loss [23]. It is defined as $\mathcal{L}_{weighted} = \ln(1 + e^{\alpha d})$, where d is the difference between a matched pair descriptor distance (Euclidean) and an unmatched pair descriptor distance, and α is a weighting factor that helps to improve convergence [13].

We also adopted a similar strategy to [28] and included bidirectional cross-domain and intra-domain ranking constraints to force the network to preserve embedding structure in both data representations. Our loss function is given in Equation 1, where \mathbf{x}_{ik} and \mathbf{y}_{ik} denote the embedded vectors (descriptors) corresponding to the k th augmentation of the map tile and panoramic image at location i , respectively, i.e. the outputs from the sub-networks in Figure 3. Note that in Equation 1, i and j refer to different locations, i.e. $1 \leq i, j \leq N$ and $i \neq j$, and k, l and m refer to the K augmentations per location, i.e. $1 \leq k, l, m \leq K$. The values of $\lambda_1, \lambda_2, \lambda_3$ and λ_4 are weighting factors to control the influence of each con-

straint in the loss function.

$$\begin{aligned}
\mathcal{L}(X, Y) = & \lambda_1 \sum_{i,j,k,l,m} \ln[1 + e^{\alpha(d(\mathbf{x}_{ik}, \mathbf{y}_{il}) - d(\mathbf{x}_{ik}, \mathbf{y}_{jm}))}] \\
& + \lambda_2 \sum_{i,j,k,l,m} \ln[1 + e^{\alpha(d(\mathbf{y}_{ik}, \mathbf{x}_{il}) - d(\mathbf{y}_{ik}, \mathbf{x}_{jm}))}] \\
& + \lambda_3 \sum_{i,j,k,l,m,k \neq l} \ln[1 + e^{\alpha(d(\mathbf{x}_{ik}, \mathbf{x}_{il}) - d(\mathbf{x}_{ik}, \mathbf{x}_{jm}))}] \\
& + \lambda_4 \sum_{i,j,k,l,m,k \neq l} \ln[1 + e^{\alpha(d(\mathbf{y}_{ik}, \mathbf{y}_{il}) - d(\mathbf{y}_{ik}, \mathbf{y}_{jm}))}]
\end{aligned} \tag{1}$$

3.5 Implementation

To train our model, we initialized Resnet50 and Resnet18 parameters with Places365 [31] and ImageNet [7] weights, respectively. The rest of the parameters in the model were initialised randomly. We fixed the weights from the first four layers of the Resnet50 network and just trained the rest of the sub-network, including NetVLAD parameters. In the map tile sub-network, we allowed all the weights to be updated, including those of Resnet18, on the basis that map tiles are quite different from ImageNet images. The number of clusters in both NetVLAD layers was 64 for all experiments.

Since the application for which we want to use the embedded space is localisation by determining which map tiles are close to a captured panoramic image (see Section 4), we placed greater emphasis on the constraint within the loss function that brings map tile descriptors for a given location closer to the corresponding panoramic descriptor, i.e. the second term in Equation 1. We found that values of $\lambda_2 = 1.0$ and $\lambda_1 = \lambda_3 = \lambda_4 = 0.2$ achieved the best results. The embedding size was set to 32 dimensions and we forced our embedded space to reside in a hypersphere manifold by performing L2-normalization on the network outputs and then scaling by a factor of 3.

The number of locations N_B in a batch was set to 20, and the number of augmentations at each location K was set to 5. Hence, in each learning step, there were 500 matched pairs and 9500 unmatched pairs. To form our triplets, we followed the batch all mining strategy discussed in [8, 12] and averaged the loss value over all possible triplets in the batch.

We trained our model for 50 epochs using the Adam

optimizer [15] with the learning rate set to 3×10^{-4} for the first 40 epochs and then reducing to 1×10^{-5} for the last 10 epochs. The value of α in Equation 1 was set to 2. We did validation every epoch and saved the model with the best recall instead of the model with the minimum loss.

4 Localisation using embedded descriptors

In this section we describe how we use the learned embedded space for geolocating panoramic images w.r.t a 2-D map. The approach is illustrated in Figure 2. The key principle is motivated by that adopted in [22]: along a route consisting of adjacent locations, the pattern of embedded descriptors obtained from the respective panoramic images enables the route to be uniquely distinguished from all other routes. The length of route required for localisation is dependent on the semantic characteristics which are reflected in both the panoramic images and 2-D map.

Localisation proceeds as follows. Given panoramic images along a route, we derive embedded descriptors via the learned model described above and compare the concatenation of the descriptors with those derived from sequences of map tiles corresponding to possible routes on the map. The closest yields the most likely route, as illustrated in Figure 2. The overall localisation methodology follows closely that in [22] and so we provide summary below and adopt similar notation for clarity.

Given an area consisting of N locations, we define a route as a set of m adjacent locations, i.e. $r_m = (l_{\gamma(1)}, l_{\gamma(2)}, \dots, l_{\gamma(m)})$, where $l_{\gamma(i)} \in L$ for $1 \leq \gamma(i) \leq N$ and thus the $\gamma(i)$, $1 \leq i \leq m$, define the route trajectory. In this work we have limited the number of possible routes by considering only routes without loops or direction reversal. We leave extension to these cases for future work. Given a panoramic image $y_{\gamma(i)}$ at location $l_{\gamma(i)}$ we extract a 4-image representation aligned with the heading direction and use the learned model to obtain an embedded descriptor $\mathbf{y}_{\gamma(i)}$. This in turn yields a route descriptor $s_m^y = (\mathbf{y}_{\gamma(1)}, \mathbf{y}_{\gamma(2)}, \dots, \mathbf{y}_{\gamma(m)})$.

Similarly, for a route within the 2-D map with locations defined by $\zeta(i)$, we can derive a route descriptor from the map tiles along the route, i.e. $s_m^x =$

$(\mathbf{x}_{\zeta(1)}, \mathbf{x}_{\zeta(2)}, \dots, \mathbf{x}_{\zeta(m)})$. Let S_m^x denote the set of such route descriptors corresponding to all routes in the map. Localisation is then defined by finding the map route \hat{r}_m whose route descriptor \hat{s}_m^x is closest to s_m^y , i.e.

$$\hat{s}_m^x = \arg \min_{s_m^x \in S_m^x} DIST(s_m^x, s_m^y) \quad (2)$$

where $DIST(s_m^x, s_m^y)$ denotes the sum of the Euclidean distances between corresponding descriptors, i.e.

$$DIST(s_m^x, s_m^y) = \sum_{i=1}^m d(\mathbf{x}_{\zeta(i)}, \mathbf{y}_{\gamma(i)}) \quad (3)$$

In practice, we apply the above minimisation each time a new panoramic image is obtained along the route being traversed, giving an estimated route and hence localisation at each time step. This raises the question as to when successful localisation has been achieved, i.e. at what route length can we have sufficient confidence in the location estimate, which we investigate in the experiments. As the results demonstrate, the length of route required for successful localisation depends on a number of factors, including the size of area being searched and the local appearance and environmental characteristics.

We also investigated the use of turn information along a route as a means of improving localisation accuracy, as adopted in [22]. Specifically, again using similar notation to that in [22], we define a binary turn pattern along a route r_m as $t_{m-1} = (t_{\gamma(1)}, t_{\gamma(2)}, \dots, t_{\gamma(m-1)})$, where the i th component of t indicates whether there is a turn between locations $l_{\gamma(i)}$ and $l_{\gamma(i+1)}$. Turn patterns can be estimated from the heading directions of the panoramic images collected along a route being traversed and computed from OSM map data. This then provides an additional constraint to that in Equation 2 in that we require the best route estimate to have a matching turn pattern to that being traversed.

Finally, note that although we adopt a brute force search approach to the above, the recursive link between routes as the length increases means that it can be efficiently implemented by careful storage and searching of route indices $\zeta(i)$. There is also significant potential for culling routes that have low matching scores at each time step and we intend to investigate this further in future work.

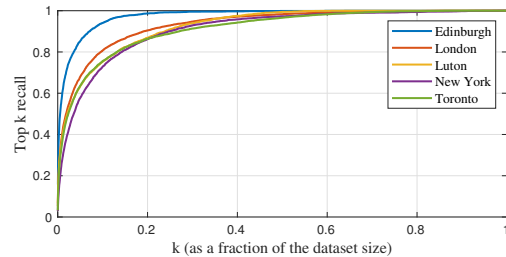


Figure 4: Top k recall of the model in the testing datasets. The horizontal axis is k given as a fraction of the dataset size and the vertical axis is the percentage of queries that were found inside the retrieved set.

Dataset	Recall @1%	Dataset	Recall @1%
Edinburgh	59.48	London	40.55
Luton	38.33	New York	27.46
Toronto	36.21		

Table 2: Top 1 % recall for 5 testing datasets.

5 Experiments

We evaluated the approach using GSV and OSM data, both the quality of the learned embedded space in terms of its ability to link location images with appropriate map tiles and the accuracy of localisation that can be achieved using embedded descriptors. We compared the latter with that achieved using binary semantic descriptors in [22].

5.1 Embedding maps and images

First, we investigated the recall performance of the embedded space when applied to the test sets, i.e. given a map tile (location image) how likely is the corresponding location image (map tile) to be the closest within the space. Results are shown in Figure 4 and Table 2, which show the top- k recall plot and the top 1% recall values, respectively. As expected, the model performs better for UK cities since the training data set contained only examples from this country and local architecture and urban layout are likely to be picked up in the learning. Note that the Luton data set also shows a considerable lower performance compared with the other UK data sets. We believe this is explained by the fact that Luton is a suburban area,



Figure 5: Top-5 retrieving examples (right) given a query image (left) in testing data sets. The green frame encloses the true map location and the blue arrow in the center of the map tile represent the position and heading.

with significant differences in appearance and layout than the urban areas used in training, and that less cartographic information is captured in OSM for such areas, leading to a mismatch between information present in the map tiles and that in the location images. However, it is interesting to note that even under these challenging conditions, our model can extract useful road information and associate it with the real topology of the road to retrieve the most probable locations. As we will show in the next section, by concatenating a consecutive number of descriptors, we are still able to localise a large number of location images correctly.

To illustrate, Figure 5 shows examples of query images and the top-5 retrieved map locations taken from different testing data sets. These demonstrate that the model has learned to relate semantics of the two domains, e.g. buildings a)-b), parks a), junctions b), rivers c), roundabouts d), among others. These results are encouraging, since they are exactly the type of features we would like to utilise for localisation. It is also interesting to see how well the learning has separated matched and unmatched image/map tile pairs in the test sets. Figure 6 shows his-

tograms of the distance between matched and unmatched pairs inside the embedding space for New York and Edinburgh. As expected, the distances between unmatched pairs tend to be larger than matched pairs, confirming that the training has been effective and is able to generalise outside the training set. Note also the smaller overlapping area for Edinburgh than New York. As we show below this improves localization accuracy and makes it less dependant on turn information.

5.2 Localisation

To evaluate the localisation, we simulated 500 routes in each of the five test cities and applied the algorithm described in Section 4. We recorded the number of routes successfully localised at every step to calculate localisation accuracy as a function of route length. We deemed a route to be successfully localised if and only if the current estimated location corresponds with the ground truth, i.e. the final location in the route.

Figure 7 shows the localisation accuracy of our method for all the test data sets for different route lengths and

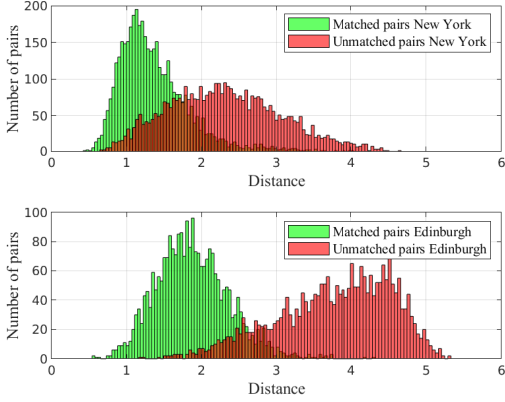


Figure 6: Histograms of distance between matched and unmatched pairs in the embedded space for New York and Edinburgh.

when using embedded descriptors only or when combining with turn patterns. Best results were obtained for London and Edinburgh, which share greater similarity with the training set, with over 90% of routes of length 20 (approximately 200m) being correctly localised. Note that turn information does not have a significant impact, especially for Edinburgh, suggesting that the embedded descriptors are encoding the turn information, further demonstrating generalisation. Accuracy is reduced for Luton, due to its different characteristics, and for cities outside of the UK, again to be expected given the environmental differences. Nonetheless, given the challenge, it is impressive that for route lengths of 20 using turn information, accuracy values above 80% are achieved for the two cities outside of the UK (Toronto also has the largest area of the test sets) and above 60% for Luton.

Figure 8 shows a comparison between our method and the binary semantic descriptor (BSD) approach described in [22]. This shows the localisation accuracy of the two methods for four different route lengths and when using descriptors alone or combining descriptors with turn patterns. We also show the accuracy achieved when only using turn patterns, i.e. matching routes based on the road pattern. We simulated BSD estimation from images, replacing the learned classifiers in [22] with bit flipping to mimic a given classification accuracy for detecting junctions and building gaps. A classification accuracy of 75%

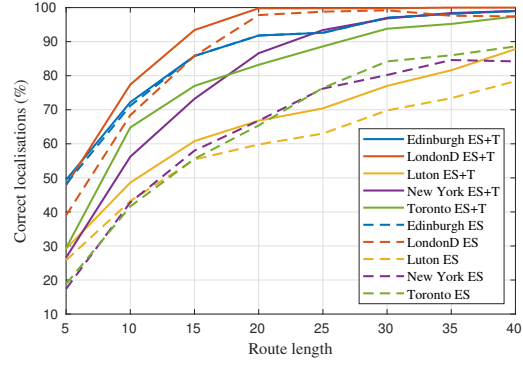


Figure 7: Route localisation accuracy versus route length for five different cities. Dashed lines indicate using only our features (ES) and solid lines indicate including turn information (ES+T).

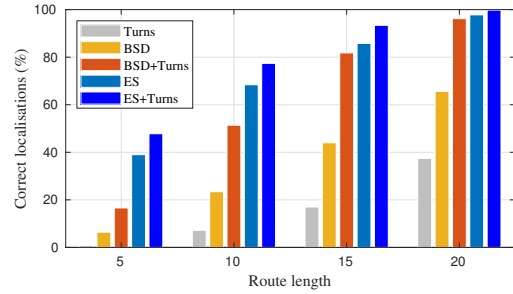


Figure 8: Localisation accuracy histograms for the London data set using our method (ES) and the BSD approach in [22] with and without turn information for different route lengths.

was used to generate the results in Figure 8, which corresponds to that reported for the learned classifiers in [22]. Our method clearly outperforms the BSD approach by a large margin. Note that it also does so without using turn information, illustrating the ability of our approach to generalise. This is further confirmed in Figure 9, which shows accuracy versus route length for New York and Luton using our method and the BSD method with different feature classification accuracy, both without turn information. Note that the latter needs to be over 80% for New York and over 90% for Luton to achieve better performance and that in both cases our method is able to successfully localise with fewer locations (shorter routes).

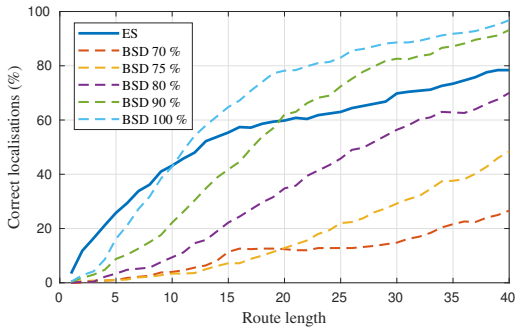
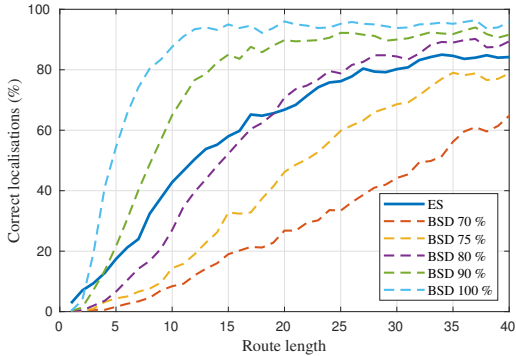


Figure 9: A comparison of accuracy localization between using our method (ES) and the BSD method in [22] for the New York (top) and Luton (bottom) data sets with different simulated accuracy values for BSD classifiers.

This is especially noticeable for Luton (bottom), which provides further evidence of generalisation given its different characteristics.

Finally, to illustrate that our model is indeed using different features than BSD, we defined a score to measure the percentage of routes that our model is correctly localising but BSD is not. Formally, let S_{BSD} and S_{ES} denote the set of routes successfully localised using BSD and ES method respectively. We define the difference score as $S_{diff} = |S_{ES} \setminus S_{BSD}| / |S_{ES}|$. A value of one would mean that none of the routes localised by our method were localised by BSD, whereas a value near zero would mean that all the successfully routes in S_{ES} are also in S_{BSD} . Results of this score for different BSD classification accuracy is shown in Fig. 10 for the Luton data set. The large values of the score at the beginning suggest that our model has been able to localize many different routes that

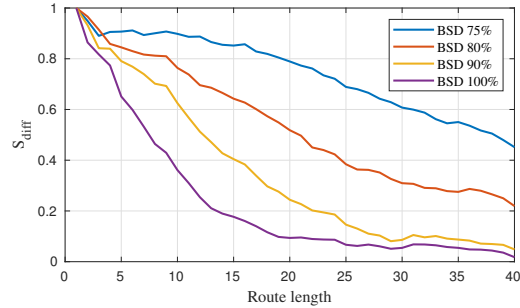


Figure 10: Relative difference score between localisation sets for our method and that in [22] for different BSD classification accuracy. High values of the score in short routes means our method is learning different semantic cues compared to BSD.

BSD has not localised, indicating that it is using more and different information.

6 Conclusions

We have presented a novel methodology to correlate 360 degree location images and 2D cartographic map tiles into a common low dimensional space using a deep learning approach. This allows us to compare both domains directly using Euclidean distance. Furthermore, we have showed how this space can be used for geolocation using an image to map matching approach. Localisation results indicate that the method can achieve up to 90 % accuracy when detecting routes of approximately 200 m length in urban areas up to 2.5 km². Moreover, the approach significantly outperforms a recent baseline method based on hand-crafted semantic features, demonstrating greater discrimination and generalisation.

References

- [1] Rosman G. Karaman S. Amini, A. and D. Rus. Variational end-to-end navigation and localization. In *Proc IEEE Int Conf on Robotics and Automation*, 2019. 3
- [2] Relja Arandjelovic, Petr Gronat, Akihiko Torii, Tomas Pajdla, and Josef Sivic. NetVLAD: CNN Architecture for Weakly Supervised Place Recognition. *IEEE Trans. on*

- Pattern Analysis and Machine Intelligence*, 40(6):1437–1451, 6 2018. 3
- [3] Anil Armagan, Martin Hirzer, Peter M. Roth, and Vincent Lepetit. Accurate camera registration in urban environments using high-level feature matching. In *Proc. British Machine Vision Conf.*, 2017. 3
- [4] Clemens Arth, Christian Pirchheim, Jonathan Ventura, Dieter Schmalstieg, and Vincent Lepetit. Instant outdoor localization and slam initialization from 2.5d maps. *IEEE Trans. on Vis. and Computer Graphics*, 21(11), 2015. 3
- [5] Marcus A. Brubaker, Andreas Geiger, and Raquel Urtasun. Map-based Probabilistic Visual Self-Localization. *IEEE Trans on Pattern Analysis and Machine Intelligence*, 38(4):652 – 665, 2016. 3
- [6] Tat-Jen Cham, Arridhana Ciptadi, Wei-Chian Tan, Minh-Tri Pham, and Liang-Tien Chia. Estimating camera pose from a single urban ground-view omnidirectional image and a 2d building outline map. *IEEE Conf. on Computer Vision and Pattern Recognition*, 2010. 3
- [7] Jia Deng, Wei Dong, Richard Socher, Li-Jia Li, Kai Li, and Li Fei-Fei. Imagenet: A large-scale hierarchical image database. In *Proc. IEEE Conf. on Computer Vision and Pattern Recognition*, pages 248–255. Ieee, 2009. 6
- [8] Shengyong Ding, Liang Lin, Guangrun Wang, and Hongyang Chao. Deep feature learning with relative distance comparison for person re-identification. *Pattern Recognition*, 48(10):2993–3003, 2015. 6
- [9] Georgios Floros, Benito van der Zander, and Bastian Leibe. Openstreetslam: Global vehicle localization using openstreetmaps. In *IEEE Int Conf on Robotics and Automation*, 2013. 3
- [10] Kaiming He, Xiangyu Zhang, Shaoqing Ren, and Jian Sun. Deep residual learning for image recognition. In *Proceedings of the IEEE Conf. on Computer Vision and Pattern Recognition*, pages 770–778, 2016. 3, 4
- [11] Simon Hecker, Dengxin Dai, and Luc Van Gool. End-to-end learning of driving models with surround-view cameras and route planners. In *Proc European Conf on Computer Vision*, 2018. 3
- [12] Alexander Hermans, Lucas Beyer, and Bastian Leibe. In defense of the triplet loss for person re-identification. *arXiv preprint arXiv:1703.07737*, 2017. 5, 6
- [13] Sixing Hu, Mengdan Feng, Rang MH Nguyen, and Gim Hee Lee. Cvm-net: Cross-view matching network for image-based ground-to-aerial geo-localization. In *Proc. IEEE Conf. on Computer Vision and Pattern Recognition*, pages 7258–7267, 2018. 3, 5
- [14] Sergey Ioffe and Christian Szegedy. Batch normalization: Accelerating deep network training by reducing internal covariate shift. *arXiv preprint arXiv:1502.03167*, 2015. 4
- [15] Diederik P Kingma and Jimmy Ba. Adam: A method for stochastic optimization. *arXiv preprint arXiv:1412.6980*, 2014. 6
- [16] T. Lin, Yin Cui, S. Belongie, and J. Hays. Learning deep representations for ground-to-aerial geolocation. In *Proc. IEEE Conf on Computer Vision and Pattern Recognition*, 2015. 3
- [17] S. Lowry, N. Sunderhauf, Paul Newman, J.J. Leonard, D. Cox, P. Corke, and M.J. Milford. Visual place recognition: A survey. *IEEE Trans on Robotics*, 32:1–19, 2016. 1
- [18] Huifang Ma, Yue Wang, Li Tang, Sarath Kodagoda, and Rong Xiong. Towards navigation without precise localization: Weakly supervised learning of goal-directed navigation cost map. *arXiv e-prints*, page arXiv:1906.02468, Jun 2019. 3
- [19] Wei-Chiu Ma, Shenlong Wang, Marcus A. Brubaker, Sanja Fidler, and Raquel Urtasun. Find your way by observing the sun and other semantic cues. In *IEEE Int Conf on Robotics and Automation*, 2017. 3
- [20] Arsalan Mousavian and Jana Kosecka. Semantic Image Based Geolocation Given a Map. *arXiv e-prints*, page arXiv:1609.00278, Sep 2016. 3
- [21] Vinod Nair and Geoffrey E Hinton. Rectified linear units improve restricted boltzmann machines. In *Proc. Int Conf on Machine Learning*, pages 807–814, 2010. 4
- [22] Pilailuck Panphattarasap and Andrew Calway. Automated map reading: Image based localisation in 2-d maps using binary semantic descriptors. In *Proc. IEEE/RSJ Int Conf on Intelligent Robots and Systems*, 2018. 1, 2, 3, 6, 7, 9, 10
- [23] F. Schroff, D. Kalenichenko, and J. Philbin. Facenet: A unified embedding for face recognition and clustering. In *2015 IEEE Conference on Computer Vision and Pattern Recognition (CVPR)*, pages 815–823, June 2015. 5
- [24] Ari Seff and Jianxiong Xiao. Learning from Maps: Visual Common Sense for Autonomous Driving. *arXiv e-prints*, page arXiv:1611.08583, Nov 2016. 3
- [25] Vincent Spruyt. Loc2vec: Learning location embeddings with triplet-loss networks. *Sentiance web article: <https://www.sentiance.com/2018/05/03/venue-mapping/>*, Accessed November 2019. 3
- [26] Yicong Tian, Chen Chen, and Mubarak Shah. Cross-view image matching for geo-localization in urban environments. In *Proc IEEE Conf on Computer Vision and Pattern Recognition*, 2017. 3
- [27] Nam N Vo and James Hays. Localizing and orienting street views using overhead imagery. In *Proc. European Conf. on Computer Vision*, pages 494–509. Springer, 2016. 3, 5

- [28] Liwei Wang, Yin Li, and Svetlana Lazebnik. Learning deep structure-preserving image-text embeddings. In *Proc. IEEE Conf. on Computer Vision and Pattern Recognition*, pages 5005–5013, 2016. 5
- [29] Scott Workman, Richard Souvenir, and Nathan Jacobs. Wide-area image geolocalization with aerial reference imagery. In *Proc. IEEE Int Conf on Computer Vision*, pages 3961–3969, 2015. 3
- [30] F. Yan, O. Vysotska, and C. Stachniss. Global localization on openstreetmap using 4-bit semantic descriptors. In *European Conf on Mobile Robots*, 2019. 3
- [31] Bolei Zhou, Agata Lapedriza, Aditya Khosla, Aude Oliva, and Antonio Torralba. Places: A 10 million image database for scene recognition. *IEEE Trans on Pattern Analysis and Machine Intelligence*, 40(6):1452–1464, 2017. 6